PHYSICAL REVIEW B **94**, 121116(R) (2016)

GWΓ + Bethe-Salpeter equation approach for photoabsorption spectra: Importance of self-consistent GWΓ calculations in small atomic systems

Riichi Kuwahara,[1,2] Yoshifumi Noguchi,[3] and Kaoru Ohno[1,*]

[1]*Department of Physics, Yokohama National University, 79-5 Tokiwadai, Hodogaya-ku, Yokohama 240-8501, Japan*
[2]*Dassault Systèmes BIOVIA K.K., ThinkPark Tower, 2-1-1 Osaki, Shinagawa-ku, Tokyo 140-6020, Japan*
[3]*Institute for Solid State Physics, The University of Tokyo, 5-1-5 Kashiwanoha, Kashiwa, Chiba 277-8581, Japan*

(Received 30 July 2015; revised manuscript received 29 June 2016; published 21 September 2016)

The self-consistent GWΓ method satisfies the Ward-Takahashi identity (i.e., the gauge invariance or the local charge continuity) for arbitrary energy (ω) and momentum ($\boldsymbol{q}$) transfers. Its self-consistent first-principles treatment of the vertex $\Gamma = \Gamma_v$ or Γ_W is possible to first order in the bare (v) or dynamically screened (W) Coulomb interaction. It is developed within a linearized scheme and combined with the Bethe-Salpeter equation (BSE) to accurately calculate photoabsorption spectra (PAS) and photoemission (or inverse photoemission) spectra (PES) simultaneously. The method greatly improves the PAS of Na, Na_3, B_2, and C_2H_2 calculated using the standard one-shot G_0W_0 + BSE method that results in significantly redshifted PAS by 0.8–3.1 eV, although the PES are well reproduced already in G_0W_0.

DOI: 10.1103/PhysRevB.94.121116

The quasiparticle (QP) equation method in many-body perturbation theory [1] is powerful for simultaneously determining the photoemission (or inverse photoemission) spectra (PES), i.e., QP energy spectra, and QP wave functions of target materials from first principles. In this method, we expand the skeleton diagrams, i.e., the diagrams drawn with the full Green's function lines, for the self-energy in terms of the electron-electron Coulomb interaction v, and solve the QP equation, which is equivalent to the Dyson equation, as a self-consistent (SC) eigenvalue problem. The Hartree-Fock (HF) approach provides the first-order approximation. In Hedin's set of equations [1], known as the GWΓ approach, the exchange-correlation part of the self-energy is expressed as $\Sigma_\sigma^{\mathrm{xc}} = iG_\sigma W\Gamma_\sigma$, where G_σ and Γ_σ are the one-particle Green's function and the vertex function (σ is the spin index), respectively, and $W = (1 - vP)^{-1}v$ represents the dynamically screened Coulomb interaction ($P = -i\sum_\sigma G_\sigma G_\sigma \Gamma_\sigma$ is the polarization function). The simplest approximation is to assume $\Gamma_\sigma = 1$, which is called the GW approximation.

It is well known that the SC GW method usually overestimates the energy gap [2,3], while the one-shot GW approach (G_0W_0) using the Kohn-Sham (KS) wave functions and eigenvalues [4] results in a better energy gap. However, quite recently, it has been pointed out that the photoabsorption spectra (PAS) for small molecules obtained by solving the Bethe-Salpeter equation (BSE) [5,6] using G_0W_0 are often significantly redshifted by about 1 eV [7,8]. The use of the Heyd-Scuseria-Ernzerhof (HSE) functional or the SC GW calculation (hereafter referred to as GW) improves the results, but they are not perfect [8,9]. For a spin-polarized sodium atom (Na) and trimer (Na_3), G_0W_0 + BSE is extremely bad, although the G_0W_0 QP energies are reasonably good [10]. The calculated and experimental [11] optical gaps for Na are 1.32 and 2.10 eV, respectively, and the calculated and experimental [12] PAS for Na_3 are shown in Fig. 1. These calculated results are far off from the experimental data [13].

Here, we develop a GWΓ method, which involves a SC treatment of the vertex $\Gamma = \Gamma_v$ or Γ_W and satisfies the Ward-Takahashi identity [14–16] to first order in v or W, and show that it remarkably improves the QP energies and the optical gaps of spin-polarized Na, Na_3,B_2, and closed-shell C_2H_2. In this method, the SC one-particle Green's function, i.e., SC QP energies and wave functions, are obtained in the GWΓ scheme. We use the all-electron mixed basis approach, in which single particle wave functions are expanded with both plane waves (PWs) and atomic orbitals (AOs) [10,17]. This Rapid Communication reports a first-principles SC GWΓ calculation and its application to the BSE, which has never been performed so far except for some recent reports of non-SC GW calculations including the second-order screened exchange by Ren *et al.* [18] and the $\mathrm{GW}\Gamma^1$ method (i.e., $\mathrm{GW}^{\mathrm{TC-TC}}$ + single-shot vertex correction for the self-energy with the static approximation) by Grüneis *et al.* [19]. All these authors used the KS, HF, or HSE wave functions throughout the calculations.

In the present SC GWΓ + BSE calculations, we will show the following: (1) Highly reliable PES and PAS are simultaneously obtained for every system. (2) All calculated results deviate by 0.1 eV at most from the available experimental data. (3) The failure of the G_0W_0 + BSE calculations for the PAS is caused by the use of localized KS wave functions above the vacuum level (VL), and hence accurate QP wave functions are required.

Except for the G_0W_0 and GW calculations, we use our recently developed technique [17] to linearize the energy dependence of the self-energy $\Sigma_\sigma(\epsilon_n)$ to avoid the non-Hermitian problem caused by the energy dependence and to perform fully SC calculations. The important point of this technique is that $\Lambda_\sigma = \lim_{(\omega,\boldsymbol{q})\to 0} \Gamma_\sigma(\boldsymbol{r}_1,\boldsymbol{r}_2,\boldsymbol{q};\mu+\omega,\mu) = 1 - \partial\Sigma_\sigma(\omega)/\partial\omega|_{\omega=\mu}$ is the vertex function in the limit $(\omega,\boldsymbol{q}) \to 0$. This is the Ward-Takahashi identity in the same limit. [Here, $\mu = (\epsilon_{\mathrm{HOMO}} + \epsilon_{\mathrm{LUMO}})/2$.] The QP equation is given by $H_\sigma|n\sigma\rangle = \epsilon_{n\sigma}\Lambda_\sigma|n\sigma\rangle$ with $H_\sigma = \hat{T} + \hat{v}_{\mathrm{nuc}} + \Sigma_\sigma(\mu) + \mu(\Lambda_\sigma - 1)$. Then, with the lower triangular matrix L_σ in the Choleski decomposition [20] $\Lambda_\sigma = L_\sigma L_\sigma^\dagger$, the renormalized QP states are given by $|\widetilde{n\sigma}\rangle = L_\sigma^\dagger|n\sigma\rangle$, which

---

[*] ohno@ynu.ac.jp

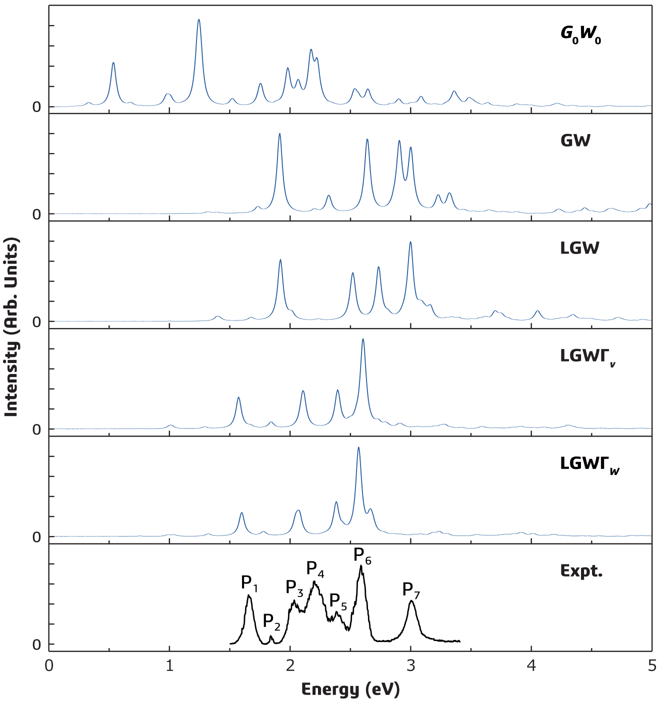

FIG. 1. Photoabsorption spectra of Na$_3$ calculated using G_0W_0, GW, LGW, LGWΓ$_v$, and LGWΓ$_W$. Experimental data are taken from Ref. [12].

satisfy $\widetilde{H}_\sigma|\widetilde{n\sigma}\rangle = \epsilon_{n\sigma}|\widetilde{n\sigma}\rangle$ with $\widetilde{H}_\sigma = L_\sigma^{-1}H_\sigma L_\sigma^{-1\dagger}$ as well as the orthogonality and completeness conditions. Moreover, the renormalized Green's function is given by $\widetilde{G}_\sigma(\omega) = L_\sigma^\dagger G_\sigma(\omega)L_\sigma$; see Ref. [17] for more details.

Theorem 1. In this linearized formulation, we can additionally introduce the vertex part $\Gamma_{v\sigma}(\boldsymbol{r}_1,\boldsymbol{r}_2,\boldsymbol{q};\epsilon+\omega,\epsilon)$ to first order in v [Fig. 2(a)], which we call the LGWΓ$_v$ method, or $\Gamma_{W\sigma}(\boldsymbol{r}_1,\boldsymbol{r}_2,\boldsymbol{q};\epsilon+\omega,\epsilon)$ to first order in W [Fig. 2(b)], which we call the LGWΓ$_W$ method. These vertex parts depend fully on the energy and momentum transfers ω and $\boldsymbol{q}$, respectively, at the center (cross in those figures). See the Supplemental Material (SM) [21] for the proof of this theorem.

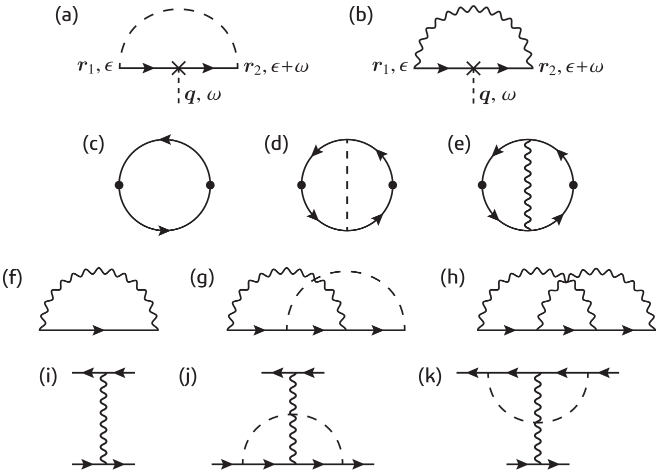

FIG. 2. Skeleton diagrams of the first-order vertex part (a) $\Gamma_{v\sigma}$ and (b) $\Gamma_{W\sigma}$; (c), (d), and (e) are the polarization part P; (f), (g), and (h) are the exchange-correlation part of the self-energy $\Sigma_\sigma^{\mathrm{xc}}$; (i), (j), and (k) are the interaction kernel $\widetilde{I}^{\sigma_1\sigma_1'}$ of the BSE. (c), (f), and (i) are usual diagrams without vertex correction; (a), (d), (g), (j), and (k) involve the first-order vertex in v (dotted line); (b), (e), and (h) involve the first-order vertex in W (wavy line).

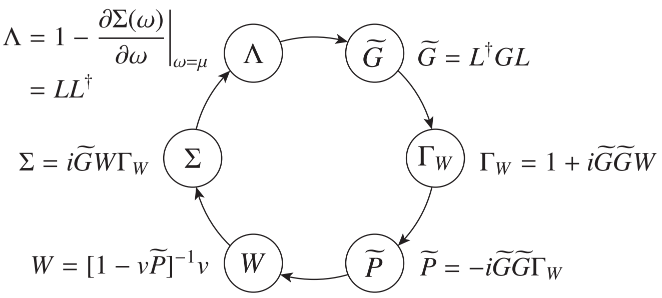

FIG. 3. Flow chart of the SC LGWΓ$_W$ method. W and Γ_W are replaced by v and Γ_v in the SC LGWΓ$_v$ method.

Then, the polarization function and the self-energy include the skeleton diagrams as shown in Figs. 2(c)–2(h). Figures 2(c) and 2(f) represent the diagrams without a vertex; Figs. 2(d) and 2(g) and Figs. 2(e) and 2(h) are the corresponding vertex corrections to first order in v ($\Gamma = \Gamma_v$) and W ($\Gamma = \Gamma_W$), respectively. Figure 3 illustrates the flow chart of the SC LGWΓ$_W$ method. The forms of the polarization function [Fig. 2(e)] and self-energy [Fig. 2(h)] are given in the SM.

Theorem 2. The present LGWΓ$_v$ and LGWΓ$_W$ methods satisfy the generalized Ward-Takahashi identity for arbitrary ω and $\boldsymbol{q}$, which is equivalent to the gauge invariance (continuity equation for the electron density) [14–16], up to first order in v and W, respectively. The proof is given in the SM.

Recently, the BSE has been solved in the one-shot second-order approach [22]. In what follows, we formulate the BSE for the LGWΓ$_v$ approach to spin-polarized systems. In the linearized formulation, we use the renormalized two-particle Green's function $\widetilde{S}^{\sigma_1\sigma_2}_{\sigma_1'\sigma_2'}(x_1,x_1';x_2,x_2') = L_{\sigma_1'}L^\dagger_{\sigma_1}S^{\sigma_1\sigma_2}_{\sigma_1'\sigma_2'}(x_1,x_1';x_2,x_2')L_{\sigma_2}L^\dagger_{\sigma_2'}$ instead of $S^{\sigma_1\sigma_2}_{\sigma_1'\sigma_2'}(x_1,x_1';x_2,x_2')$, defined by subtracting $\delta_{\sigma_1\sigma_1'}\delta_{\sigma_2\sigma_2'}G(x_1,x_1')G(x_2,x_2')$ from the original two-particle Green's function. It satisfies the BSE

$$\begin{aligned}\widetilde{S}^{\sigma_1\sigma_2}_{\sigma_1'\sigma_2'}&(x_1,x_1';x_2,x_2')\\ &= \widetilde{G}_{\sigma_1}(x_1,x_2)\widetilde{G}_{\sigma_1'}(x_2',x_1')\delta_{\sigma_1'\sigma_2'}\delta_{\sigma_1\sigma_2}\\ &\quad + \sum_{\sigma_4\sigma_4'}\int \widetilde{G}_{\sigma_1}(x_1,x_3)\frac{\delta\Sigma_{\sigma_3\sigma_3'}(x_3,x_3')}{\delta\widetilde{G}_{\sigma_4\sigma_4'}(x_4,x_4')}\widetilde{G}_{\sigma_1'}(x_3',x_1')(L_{\sigma_4'}L^\dagger_{\sigma_4})^{-1}\\ &\quad \times \widetilde{S}^{\sigma_4\sigma_2}_{\sigma_4'\sigma_2'}(x_4,x_4';x_2,x_2')d^4x_3d^4x_3'd^4x_4d^4x_4', \end{aligned} \tag{1}$$

where we used the fact that the original kernel $\Xi^{\sigma_3\sigma_4}_{\sigma_3'\sigma_4'}(x_3,x_3';x_4,x_4')$ is given by

$$\Xi^{\sigma_3\sigma_4}_{\sigma_3'\sigma_4'} = \frac{\delta\Sigma_{\sigma_3\sigma_3'}}{\delta G_{\sigma_4\sigma_4'}} = \frac{\delta\widetilde{G}_{\sigma_3\sigma_3'}}{\delta G_{\sigma_3\sigma_3'}}\frac{\delta\Sigma_{\sigma_3\sigma_3'}}{\delta\widetilde{G}_{\sigma_4\sigma_4'}} = L_{\sigma_3}\frac{\delta\Sigma_{\sigma_3\sigma_3'}}{\delta\widetilde{G}_{\sigma_4\sigma_4'}}L^\dagger_{\sigma_3'}. \tag{2}$$

The functional derivative $\delta\Sigma_{\sigma_3\sigma_3'}(x_3,x_3')/\delta\widetilde{G}_{\sigma_4\sigma_4'}(x_4,x_4')$ is given by $-i\delta_{\sigma_3\sigma_3'}\delta_{\sigma_4\sigma_4'}\delta(x_3-x_3')\delta(x_4-x_4')v(\boldsymbol{r}_3-\boldsymbol{r}_4)+\delta_{\sigma_3\sigma_4}\delta_{\sigma_3'\sigma_4'}\widetilde{I}^{\sigma_3\sigma_3'}(x_3,x_3';x_4,x_4')$. Ignoring all terms having functional derivatives of $W[\widetilde{G}]$ with respect to $\widetilde{G}$ as usual [23], we have $\widetilde{I}^{\sigma_3\sigma_3'}(x_3,x_3';x_4,x_4')$ expressed as $i\{\delta(x_3-x_4)\delta(x_3'-$

$x_4')W(x_3,x_3') + \delta(x_3 - x_4)[W\Gamma_{v\sigma_3'}](x_3',x_4';x_3) + \delta(x_3' - x_4')[W\Gamma_{v\sigma_3}](x_3,x_4;x_3')\}$, which is represented by the skeleton diagrams of Figs. 2(i), 2(j), and 2(k). Here the last two terms [Figs. 2(j) and 2(k)] come from vertex correction to first order in v. From these equations, we find that $\Lambda_\sigma = L_\sigma \underset{\sim}{L}_\sigma^\dagger$ should be multiplied to the polarization function as $\widetilde{P}^\sigma_{\boldsymbol{GG}'} = P^\sigma_{\boldsymbol{GG}'}\Lambda_\sigma$ [17]. Then, putting $V^{\sigma_1\sigma_2}_{\nu\mu dc} = \sum_{\boldsymbol{G}} \langle \widetilde{\nu\sigma_1}|e^{i\boldsymbol{G}\cdot\boldsymbol{r}}|\widetilde{\mu\sigma_1}\rangle\langle d\sigma_2|e^{-i\boldsymbol{G}\cdot\boldsymbol{r}'}|c\sigma_2\rangle v(\boldsymbol{G})$ and using the expression for $\widetilde{I}^{\sigma_1\sigma_1'}_{\nu\mu dc}(\omega)$ given in the SM, we obtain the matrix eigenvalue equation of the BSE [23],

$$(\epsilon_{c'\sigma_1} - \epsilon_{d'\sigma_1'} - \Omega_r)A^r_{d'\sigma_1',c'\sigma_1} = -\sum_d^{\text{occ}}\sum_c^{\text{emp}}\left\{\delta_{\sigma_1\sigma_1'}\sum_{\sigma_2} V^{\sigma_1\sigma_2}_{c'd'dc}A^r_{d\sigma_2,c\sigma_2} - \widetilde{I}^{\sigma_1\sigma_1'}_{c'd'dc}(\Omega_r)A^r_{d\sigma_1',c\sigma_1}\right\}, \tag{3}$$

in the Tamm-Dancoff approximation [23]. We also use this formulation in the LGWΓ$_W$ approach, because the resulting error is on the order of 0.01 eV.

For spin-polarized systems, we have to generally solve the eigenvalue equation (3) in the ↑↑-↓↓ subspace,

$$\begin{pmatrix} h^{\uparrow\uparrow} + v^{\uparrow\uparrow} & v^{\uparrow\downarrow} \\ v^{\downarrow\uparrow} & h^{\downarrow\downarrow} + v^{\downarrow\downarrow} \end{pmatrix}\begin{pmatrix} A^r_{\uparrow\uparrow} \\ A^r_{\downarrow\downarrow} \end{pmatrix} = 0, \tag{4}$$

where we put $h^{\sigma_1\sigma_1'} = (\epsilon_{c'\sigma_1} - \epsilon_{d'\sigma_1'} - \Omega_r)\delta_{cc'}\delta_{dd'} - \widetilde{I}^{\sigma_1\sigma_1'}_{c'd'dc}$ and $v^{\sigma_1\sigma_2} = V^{\sigma_1\sigma_2}_{c'd'dc}$.

We used a face-centered-cubic unit cell with edge length of 14 Å for Na and B_2, 15 Å for C_2H_2, and 18 Å for Na_3. All of the core and (truncated) valence numerical AOs are used together with the PWs. The atomic geometries are optimized with DMol^3 [24,25]. The bond lengths are 3.23, 3.23, and 5.01 Å for Na_3, 1.61 Å for B_2, 1.20 Å for C≡C, and 1.06 Å for C-H at the Becke three-parameter Lee-Yang-Parr (B3LYP) functional level. We used 3.61 (50.76) Ry, 1.23 (30.7) Ry, 6.82 (38.1) Ry, and 11.1 (44.2) Ry cutoff energies for PWs (for Σ^x_σ), respectively, for Na, Na_3, B_2, and C_2H_2. The cutoff energy for P and Σ^c_σ is the same as that for PWs for Na and Na_3, and is set at 4.57 Ry for B_2 and 3.98 Ry for C_2H_2. We used the full ω integration [26] and the projection operator for the GW-related calculations, but used the plasmon-pole model [27] and 600 empty states for the Γ-related calculations as well as for solving the BSE in order to save the computational cost.

The resulting ionization potential (IP), electron affinity (EA), and optical gap E_g^{opt} (corresponding to the first dipole-allowed transition) of Na, Na_3, B_2, and C_2H_2 calculated using the G_0W_0, GW, LGW, and LGWΓ$_W$ methods are listed in Tables I and II, together with the results of previous multireference single and double configuration interaction (MRDCI) calculations [28–34], configuration interaction single and double (CID) calculations [35], and the corresponding experimental values [11,12,36–45]. For Na and Na_3, the results of LGWΓ$_v$ are also listed in Table I. Note that EA of C_2H_2 is negative and not shown in Table II. Let us first compare the results of IP and EA with the experimental values. G_0W_0 results in reasonable IP and EA (IP of C_2H_2 is similar to those obtained in Ref. [46]) while GW has a tendency to overestimate IP and underestimate EA, although the experimental error bar is large for B_2. LGW improves GW [17], but is not perfect. In contrast, LGWΓ$_v$ and LGWΓ$_W$ almost perfectly improve both IP and EA. For LGWΓ$_W$, the deviation from the experimental values is 0.03 eV for Na, 0.07 eV for Na_3, and 0.01 eV for C_2H_2. Compared with previous MRDCI calculations, [28–32,34] our results are closer to the experimental IP and EA for almost all cases.

Next we compare the results of the optical gap E_g^{opt} with experiments. G_0W_0 significantly underestimates the experimental E_g^{opt} for all systems and GW overestimates

TABLE I. Ionization potential (IP), electron affinity (EA), and optical gap E_g^{opt} (corresponding to $^2S \rightarrow {}^2P$ and $^2B_2 \rightarrow {}^2A_1$ transitions) of Na and Na_3 (in units of eV).

	Na			Na_3		
	IP	EA	E_g^{opt}	IP	EA	E_g^{opt}
G_0W_0	5.15	0.41	1.32	4.10	1.14	0.53
GW	5.40	0.33	2.23	4.64	0.51	1.91
LGW	5.23	0.42	2.18	4.48	0.66	1.92
LGWΓ$_v$	5.01	0.60	2.00	4.08	1.04	1.57
LGWΓ$_W$	5.12	0.58	2.16	4.04	1.15	1.60
MRDCI	4.97[a]	0.44[b]	1.98[b]	3.76[c]	1.07/1.17[b]	1.61[b]
Expt.	5.14[d]	0.55[e]	2.10[f]	3.97[g]	1.02/1.16[h]	1.65[i]

[a] Reference [28].
[b] Reference [29].
[c] Reference [30].
[d] Reference [36].
[e] Reference [37].
[f] Reference [11].
[g] Reference [38].
[h] Reference [39].
[i] Reference [12].

TABLE II. IP, EA, and E_g^{opt} (corresponding to the $^3\Sigma_g^- \rightarrow {}^3\Sigma_u^-$ transition) of B_2, and IP and E_g^{opt} (corresponding to the $^1\Sigma_g^+ \rightarrow {}^1\Pi_u$ transition) of C_2H_2 (in units of eV).

	B_2			C_2H_2	
	IP	EA	E_g^{opt}	IP	E_g^{opt}
G_0W_0	9.21	2.18	2.44	11.05	5.01
GW	9.97	1.76	3.94	11.65	8.39
LGW	9.79	1.94	3.75	11.44	8.23
LGWΓ$_W$	9.87	1.91	3.84	11.48	8.25
MRDCI	9.48[a]	2.0[b]	3.85[c]	11.21[d]	(8.06)[e]
Expt.	10.3±0.6[f]	1.8±0.4[g]	3.79[h]	11.49[i]	8.16[j]

[a] Reference [31].
[b] Reference [32].
[c] CASSCF/MRDCI: Ref. [33].
[d] Reference [34].
[e] CID: Ref. [35].
[f] Reference [40].
[g] Reference [41].
[h] References [42,43].
[i] Reference [44].
[j] Reference [45].

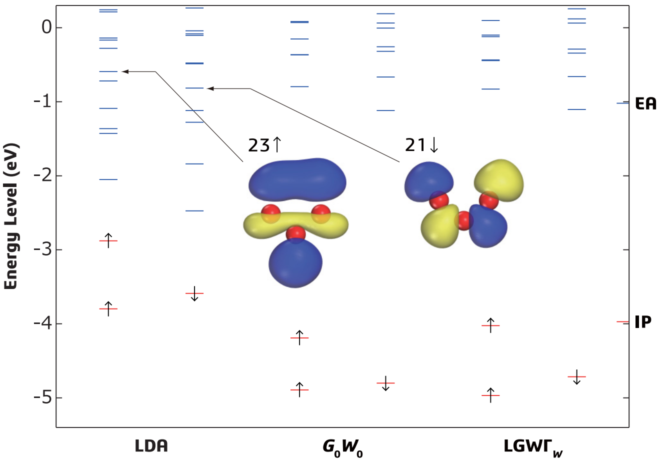

FIG. 4. QP (or KS) energy spectra of Na_3 calculated using the LDA, G_0W_0, and LGWΓ_W. Unphysically bound KS wave functions at the 21st spin-down level and the 23rd spin-up level are also depicted. Red balls are Na atoms, while yellow and blue indicate the positive and negative regions of the wave function, respectively.

the experimental E_g^{opt}. The deviation from the experimental values is 0.8–3.1 eV for G_0W_0 and 0.13–0.26 eV for GW. LGW improves the results except for Na_3; the deviation from the experimental values is 0.08 eV for Na, 0.27 eV for Na_3, 0.04 eV for B_2, and 0.07 eV for C_2H_2. In contrast, LGWΓ_v and LGWΓ_W give excellent E_g^{opt} for all systems. For LGWΓ_W, the difference between the theoretical and experimental values is less than 0.06 eV for Na and Na_3, 0.05 eV for B_2, and 0.09 eV for C_2H_2. Compared with the experimental values, our E_g^{opt} is better than the previous MRDCI results for Na [29], and CID results for C_2H_2 [35], or comparable to (differs only by 0.01 eV from) previous MRDCI results for Na_3 [29], and complete-active-space self-consistent-field (CASSCF)/MRDCI results for B_2 [33]. The LGWΓ_W + BSE photoabsorption peak, i.e., the exciton wave function, mainly consists of the following QP hole and electron level pair(s): $6(s\uparrow) \rightarrow 7(p\uparrow)$ for Na, $17(s\uparrow) \rightarrow 19(p\uparrow)$ for Na_3, $4(\sigma\uparrow) \rightarrow 7(\pi\uparrow)$ and $3(\sigma\downarrow) \rightarrow 6(\pi\downarrow)$ for B_2, and $7(\pi) \rightarrow 8(\sigma)$ for C_2H_2. Figure 1 shows the PAS of Na_3 calculated using G_0W_0, GW, LGW, LGWΓ_v, and LGWΓ_W and the experimental spectra [12]. The overall spectral shapes are similar in all these methods except for G_0W_0, although the peak positions are almost constantly shifted by an amount indicated by the difference between the calculated and experimental E_g^{opt}'s in Table I, and the peak heights somewhat change after the inclusion of the vertex correction. Obviously, GW and LGW overestimate the peak positions, while LGWΓ_v and LGWΓ_W give good peak positions except for P_4 and P_7. (LGWΓ_v has a small peak at 2.9 eV, which may correspond to P_7.) The remaining discrepancy between the theory and experiment in the case of Na_3 may be mainly attributed to the neglect of isomers and the atomic vibration effects.

Figure 4 shows the QP (or KS) energy spectra calculated using the local density approximation (LDA), G_0W_0, and LGWΓ_W. The experimental IP and EA are indicated by IP and EA on the right vertical border line. Now we discuss the reason why the PAS calculated using G_0W_0 + BSE are so poor. For Na_3, the number of up-spin (down-spin) levels below the VL is 26 (26) for LDA, 20 (19) for GW, 20 (20) for LGW, and 22 (20) for LGWΓ_v and LGWΓ_W. We confirmed that the KS and QP wave functions very much resemble each other for the first 20 levels below the VL. However, they are quite different for the QP levels above the VL. For example, the spin-up and spin-down KS wave functions at the 21st down-spin level and the 23rd up-spin level below the VL are depicted in Fig. 4. They are localized. However, the corresponding G_0W_0 QP energies are both above the VL and the full QP wave functions are not localized. In our G_0W_0 + BSE calculation of Na_3, the first small photoabsorption peak around 0.35 eV (see the top panel in Fig. 1) mainly consists of the QP hole and electron level pairs between $16 \rightarrow 17$ (19.8%), 21 (8.7%) for down spin, and $17 \rightarrow 18$ (21.8%), 20 (31.4%), 21 (9.0%), 23 (2.3%) for up spin. The unphysically bound KS wave functions of the 21↓ and 23↑ levels contribute to the BSE matrix elements, leading to unphysically large electron-hole interactions and, in turn, to the optical transitions with very small photoabsorption energies. This gives the wrong spectra for G_0W_0 in Fig. 1. It has already been known for more than 50 years [47] that the BSE should be solved with the fully SC Green's function in order to satisfy the conservation laws as well as the longitudinal f-sum rule. However, the QP gap and the optical gap obtained using the GW method are blueshifted because they do not satisfy the generalized Ward-Takahashi identity. To improve the result, it is necessary to use the GWΓ method.

In this Rapid Communication, we presented the G_0W_0, GW, LGW, and LGWΓ_W (LGWΓ_v) calculations for Na, Na_3, B_2, and C_2H_2. If the G_0W_0 QP energies are used together with the KS wave functions, there is inconsistency between the QP energies and wave functions at some levels above the VL. Moreover, the GW and LGW methods are not sufficient because they overestimate both the QP energy gap and optical gap. To obtain better gap estimates, it is necessary to perform the GWΓ calculation. We showed that the LGWΓ_W method produces consistent and the best PES and PAS among all of the methods used in this study. The self-consistent treatment of Γ is required to obtain consistently good results for both PES and PAS, and its computational cost scales as $O(N^2M^3)$, where N and M are the numbers of basis functions and empty states, respectively, if we use the plasmon-pole model. The present method is applicable to vertical transitions but cannot handle relaxation processes.

This work was supported by the Grant-in-Aid for Scientific Research B (Grant No. 25289218) from JSPS and also by the Grant-in-Aid for Scientific Research on Innovative Areas (Grant No. 25104713) from MEXT. We are also indebted to the HPCI promoted by MEXT for the use of the supercomputer SR16000 at Hokkaido University and at IMR, Tohoku University (Project IDs No. hp140214, No. hp150231, No. hp160072, and No. hp160234).

[1] L. Hedin, Phys. Rev. **139**, A796 (1965).

[2] T. Kotani, M. van Schilfgaarde, and S. V. Faleev, Phys. Rev. B **76**, 165106 (2007).

[3] M. Shishkin, M. Marsman, and G. Kresse, Phys. Rev. Lett. **99**, 246403 (2007).

[4] M. S. Hybertsen and S. G. Louie, Phys. Rev. Lett. **55**, 1418 (1985).

[5] G. Onida, L. Reining, R. W. Godby, R. Del Sole, and W. Andreoni, Phys. Rev. Lett. **75**, 818 (1995).

[6] M. Rohlfing and S. G. Louie, Phys. Rev. Lett. **80**, 3320 (1998).

[7] D. Hirose, Y. Noguchi, and O. Sugino, Phys. Rev. B **91**, 205111 (2015).

[8] D. Jacquemin, I. Duchemin, and X. Blase, J. Chem. Theory Comput. **11**, 3290 (2015).

[9] F. Bruneval, S. M. Hamed, and J. B. Neaton, J. Chem. Phys. **142**, 244101 (2015).

[10] Y. Noguchi, S. Ishii, K. Ohno, and T. Sasaki, J. Chem. Phys. **129**, 104104 (2008).

[11] J. E. Sansonetti, J. Phys. Chem. Ref. Data **37**, 1659 (2008).

[12] C. R. C. Wang, S. Pollack, T. A. Dahlseid, G. M. Koretsky, and M. M. Kappes, J. Chem. Phys. **96**, 7931 (1992).

[13] For the even number clusters of sodium, the G_0W_0 + BSE result is not that bad; see Ref. [5] and Y. Noguchi and K. Ohno, Phys. Rev. A **81**, 045201 (2010).

[14] J. C. Ward, Phys. Rev. **78**, 182 (1950).

[15] Y. Takahashi, Il Nuovo Cimento **6**, 371 (1957).

[16] J. R. Schrieffer, *Theory of Superconductivity* (Westview Press, Boulder, CO, 1999), Chap. 8-5.

[17] R. Kuwahara and K. Ohno, Phys. Rev. A **90**, 032506 (2014).

[18] X. Ren, P. Rinke, G. E. Scuseria, and M. Scheffler, Phys. Rev. B **88**, 035120 (2013).

[19] A. Grüneis, G. Kresse, Y. Hinuma, and F. Oba, Phys. Rev. Lett. **112**, 096401 (2014).

[20] It is also possible to use $L = \Lambda^{1/2}$ instead of the Choleski decomposition in the linearization procedure as in Ref. [3].

[21] See Supplemental Material at http://link.aps.org/supplemental/10.1103/PhysRevB.94.121116 for the proof of Theorem 1 and Theorem 2.

[22] D. Zhang, S. N. Steinmann, and W. Yang, J. Chem. Phys. **139**, 154109 (2013).

[23] G. Strinati, Phys. Rev. Lett. **49**, 1519 (1982).

[24] B. Delley, J. Chem. Phys. **92**, 508 (1990).

[25] B. Delley, J. Chem. Phys. **113**, 7756 (2000).

[26] M. Zhang, S. Ono, N. Nagatsuka, and K. Ohno, Phys. Rev. B **93**, 155116 (2016).

[27] W. von der Linden and P. Horsch, Phys. Rev. B **37**, 8351 (1988).

[28] R. J. Buenker and S. Krebs, in *Recent Advances in Multireference Methods*, edited by K. Hirao, Recent Advances in Computational Chemistry Vol. 4 (World Scientific, Singpaore, 1999), pp. 1–29.

[29] V. Bonačić-Koutecký, P. Fantucci, and J. Koutecký, J. Chem. Phys. **93**, 3802 (1990).

[30] V. Bonačić-Koutecký, I. Boustani, M. Guest, and J. Koutecký, J. Chem. Phys. **89**, 4861 (1988).

[31] P. J. Bruna and J. S. Wright, J. Phys. Chem. **94**, 1774 (1990).

[32] P. J. Bruna and J. S. Wright, J. Phys. B **23**, 2197S (1990).

[33] S. R. Langhoff and C. W. Bauschlicher, Jr., J. Chem. Phys. **95**, 5882 (1991).

[34] W. P. Kraemer and W. Koch, Chem. Phys. Lett. **212**, 631 (1993).

[35] W. E. Kammer, Chem. Phys. **5**, 408 (1974).

[36] A. Herrmann, E. Schumacher, and L. Wöste, J. Chem. Phys. **68**, 2327 (1978).

[37] H. Hotop and W. C. Lineberger, J. Phys. Chem. Ref. Data **14**, 731 (1985).

[38] A. Herrmann, S. Leutwyler, E. Schumacher, and L. Woste, Helv. Chim. Acta **61**, 453 (1978).

[39] K. M. McHugh, J. G. Eaton, G. H. Lee, H. W. Sarkas, L. H. Kidder, J. T. Snodgrass, M. R. Manaa, and K. H. Bowen, J. Chem. Phys. **91**, 3792 (1989).

[40] L. Hanley, J. L. Whitten, and S. L. Anderson, J. Phys. Chem. **92**, 5803 (1988).

[41] C. J. Reid, Int. J. Mass Spectrosc. Ion Process. **127**, 147 (1993).

[42] W. R. M. Graham and W. Weltner, Jr., J. Chem. Phys. **65**, 1516 (1976).

[43] K. P. Huber and G. Herzberg, *Molecular Spectra and Molecular Structure: IV. Constants of Diatomic Molecules* (Van Nostrand Reinhold, New York, 1979).

[44] G. Bieri and L. Åsbrink, J. Electron Spectrosc. Relat. Phenom. **20**, 149 (1980).

[45] W. C. Price, Phys. Rev. **47**, 444 (1935).

[46] M. J. van Setten, F. Caruso, S. Sharifzadeh, X. Ren, M. Scheffler, F. Liu, J. Lischner, L. Lin, J. R. Deslippe, S. G. Louie, C. Yang, F. Weigend, J. B. Neaton, F. Evers, and P. Rinke, J. Chem. Theory Comput. **11**, 5665 (2015).

[47] G. Baym and L. P. Kadanoff, Phys. Rev. **124**, 287 (1961).